Evolution of DNA compaction in microchannels

2006 J. Phys.: Condens. Matter 18 S639

(http://iopscience.iop.org/0953-8984/18/18/S10)

INSTITUTE OF PHYSICS PUBLISHING JOURNAL OF PHYSICS: CONDENSED MATTER

J. Phys.: Condens. Matter **18** (2006) S639–S652 doi:10.1088/0953-8984/18/18/S10

Evolution of DNA compaction in microchannels

Rolf Dootz[1], Alexander Otten[2], Sarah Köster[1], Bernd Struth[3] and Thomas Pfohl[1,4]

[1] Max Planck Institute for Dynamics and Self-Organization, Bunsenstraße 10, 37073 Göttingen, Germany
[2] Applied Physics Department, University of Ulm, Albert-Einstein-Allee 11, 89069 Ulm, Germany
[3] European Synchrotron Radiation Facility, 6 rue Horovitz, BP 220, 38043 Grenoble, France

E-mail: thomas.pfohl@ds.mpg.de

Received 17 August 2005, in final form 4 January 2006
Published 19 April 2006
Online at stacks.iop.org/JPhysCM/18/S639

Abstract

Combining microfluidics with x-ray microdiffraction and Raman microscopy, the dynamic behaviour of soft matter, with specific consideration of the molecular structure, can be investigated. Microfluidic systems enable a reduction of sample volume and shorter reaction times. By performing experiments under continuous microflow, material damage is avoided and the influence of external stress on biomacromolecules can be analysed. The generated elongated flow induces alignment of the investigated materials, allowing for an improved structural characterization. Here, the dynamics of the compaction of DNA by polypropyleneimine dotriacontaamine dendrimers, generation 4 is studied. As a consequence of the laminar flow inside the microchannels, highly defined, diffusion-controlled compaction of the DNA occurs enabling the study of different states of the reaction during one measurement by varying the observation position in the channels. The evolution of a columnar mesophase with an in-plane square symmetry is monitored by x-ray microdiffraction and the molecular interaction between the two reactants is traced using Raman microscopy, leading to a more profound comprehension of the condensation reaction. The experimental results are in accordance with finite element method simulations of the flow and diffusion profiles in the elongated flow device.

(Some figures in this article are in colour only in the electronic version)

1. Introduction

DNA condensation represents the process by which the genetic information is packed and protected. Sophisticated and reversible packing mechanisms *in vivo* enable tasks such as

[4] Author to whom any correspondence should be addressed.

replication or transcription. Moreover, DNA condensation provides a promising means whereby DNA containing genes of therapeutic interest can be prepared for transfer from solution to target cells. From a more physical point of view, it represents a demanding problem of phase transition, liquid crystal behaviour and polyelectrolyte interaction. A profound knowledge of the DNA organizing factors is needed to understand processes such as replication or transcription which are crucially dependent on DNA packing.

DNA condensation *in vivo* is promoted by DNA-binding proteins [1–3] but also by molecular crowding leading to concentrations as high as 800–1000 mg ml^{-1} in viral heads or sperm cells [4]. To reduce the repulsion between DNA segments, multivalent counterions (e.g. spermidine) are involved [5, 6]. Because of their importance in the compaction of DNA *in vivo*, we want to focus on the condensation of DNA by multivalent polycations. This is primarily driven by electrostatic interactions and entropic gains derived upon the release of bound counterions [7–9] and reorganization of the water molecules surrounding the DNA surface [10]. When the concentration of multivalent ions is raised above a certain threshold, a rapid aggregation of DNA segments into (neutral) bundles results, and these precipitate from the solution [11]. The remaining interactions between the neutral polyplexes will generally be attractive and promote further aggregation into bigger clusters.

One of the currently most discussed classes of polyplexes is dendrimer/DNA. Dendrimers, a new class of monodisperse synthezizable particles with tuneable characteristics, have a treelike molecular architecture characterized by regular dendritic branching with radial symmetry. The spherical shape is achieved by successively attaching polymer subunits around an initiator core. The well-defined size and the charge distribution of the molecule are determined by the number of layers or generations present in the polymer. Depending on their generation, their diameter may be up to tens of nanometres.

Dendrimers are capable of self-organizing into superstructures [12, 13]. The repeating structural units of dendrimers can be chemically modified, resulting in a variety of supramolecular structures. These characteristics suggest possible utilization of dendrimers for binding DNA. Dendrimers show high efficiency as transfection vectors [14–16] and stabilize the transfected genetic material inside the cell and may therefore prolong its survival *in vivo* and increase the probability of genomic recombination [1, 17]. Furthermore, analysing DNA compaction by dendrimers, which act as model histones or histone-like proteins (DPS, etc), can help to gain deeper insights into the (hierarchical) organisation of DNA *in vivo*. As with other polycations, the exact mechanisms involved in transfection using dendrimers are not fully understood. Thus, more detailed information on the interactions between DNA and dendrimers is required. To study the interaction between DNA and dendrimers we use a microscale hydrodynamic focusing system.

Recently, remarkable progress has been achieved in the integration and analysis of chemical and biological processes at the nanolitre scale by using microfluidic handling systems [18–20]. These microfluidic systems enable the reduction of sample volumes and shorter reaction and analysis times. Furthermore, owing to the interesting physics of fluid flow on the microscale, microfluidics is a powerful tool for the investigation of soft condensed matter [21, 22]. Sizing the microchannels to dimensions comparable to those inside the cell nucleus or viral capsids gives an insight to the behaviour of DNA in living systems. By performing experiments under continuous flow inside microfluidic devices, the influence of external stress on biomacromolecules can be analysed and the molecules can be oriented. Showing generally poor interpretative features when unoriented, hydrodynamic focusing leads to highly ordered structures which allow for an efficient characterization of biomacromolecular systems. Due to the laminar flow inside the microchannels, the compaction of the DNA is diffusion controlled allowing the compaction of the DNA to occur in a highly defined way.

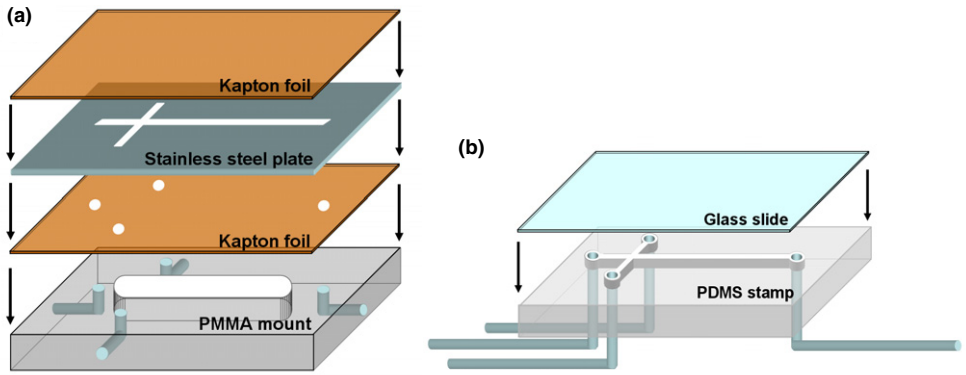

Figure 1. Schematic of the flow cells used: (a) stainless steel cells for x-ray microdiffraction, (b) PDMS cells for Raman microscopy.

Thereby, the formation of kinetically trapped structures different from thermodynamically favoured conformations (hexagonally packed, curved toroidal, etc [23, 24]) is minimized and more compact and ordered condensates are formed in the microchannels. Study of different states of the reaction during one measurement is possible by varying the observation position and the flow velocities in the channels.

In this paper we describe hydrodynamic focusing experiments with DNA and dendrimer/DNA condensates, which are investigated by small angle x-ray microdiffraction in microscale channels. Focusing the x-ray beams down to the micrometre scale offers the ability to characterize the influence of microscale confinement on the nanoscale structures of the condensed biomaterials used [25]. As a complement to small angle x-ray scattering we use confocal Raman microscopy to visualize the hydrodynamically focused reactant species. Being a rapid, non-destructive, chemically sensitive method of imaging, Raman microscopy is independent of additional marker molecules and provides a large lateral resolution enabling quantitative analysis and *in situ* detection. By performing the experiments under continuous flow inside our microfluidic devices damage to the sample is avoided. The combination of both the structural information resulting from small angle x-ray scattering measurements and the chemical sensitivity of Raman imaging allows for a detailed insight into the characteristics and dynamics of the self-assembled, supramolecular G4/DNA condensates.

2. Materials and methods

2.1. Microfluidic devices

The microfluidic devices for hydrodynamic focusing and diffusive mixing consist of flow chambers with two crossed rectangular microchannels (figure 1). For x-ray microdiffraction experiments, perpendicularly crossing channels with a width of 100–150 μm and a depth of 200–300 μm are spark eroded into stainless steel plates. The top and bottom surfaces of the plates are covered by thin, self-adhesive Kapton foils (foil thickness $\approx$20 μm). Four holes are punched into the bottom Kapton foils fitting the channel ends of the steel plates. The Kapton–steel–Kapton system is mounted onto a poly(methylmethacrylate) (PMMA) support with corresponding connections to the channel ends. The centre region of the PMMA support is milled out to provide an undisturbed pathway for x-ray beams. The PMMA support is connected to a pumping system by Teflon tubing (figure 1(a)).

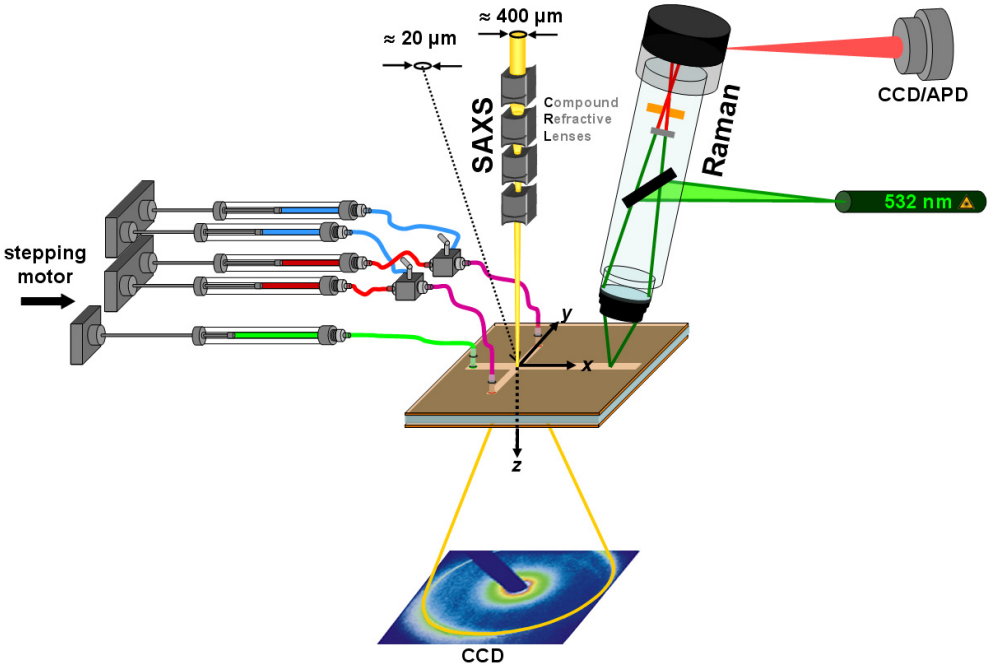

Figure 2. Schematic of the experimental setup.

For Raman measurements, the microchannels are fabricated using standard soft lithography techniques [26]. This method involves casting of non-crosslinked Sylgard 184 poly-(dimethylsiloxane) (PDMS, purchased from Dow Corning) against a master with a relief structure consisting of SU 8-50 photoresist (MicroChem). The microchannels in the cross-linked PDMS stamp are sealed with a glass slide (figure 1(b)) [22].

The pumping system utilizes five microlitre syringes, one for the main channel and two for each of the two side channels, which are connected via a T-junction. In our setup, aqueous solutions of polydisperse DNA sodium salt highly polymerized from calf thymus with an average length of 5 μm (purchased from Sigma Aldrich) are injected into the centre channel and hydrodynamically focused by pure water streams from the side channels (figure 2). After establishing a stationary flow, monodisperse polypropyleneimine dotriacontaamine dendrimer, generation 4.0 (G4, purchased from Sigma Aldrich) are continuously added to both side streams via the T-junction with the second set of syringes (figure 2). By varying the co-flow in the side channels, the concentration of the reactants during the measurement can be adjusted. The step motor used for flushing the syringes is controlled by a Lab View computer interface. The custom-made syringe pumps allow for a continuous pumping at very low flow rates (10^{-9} l s^{-1}). The resulting experimental flow velocities are between ≈100 and ≈2000 μm s^{-1}.

2.2. Small angle x-ray microdiffraction

The small angle x-ray microdiffraction experiments are conducted at beam line ID10B at the European Synchrotron Radiation Facility (ESRF) [25, 27]. A schematic illustration of the experimental setup is shown in figure 2. The microfluidic device is mounted onto a goniometer and the x-ray beam is adjusted by using focusing optics. Beryllium compound refractive lenses

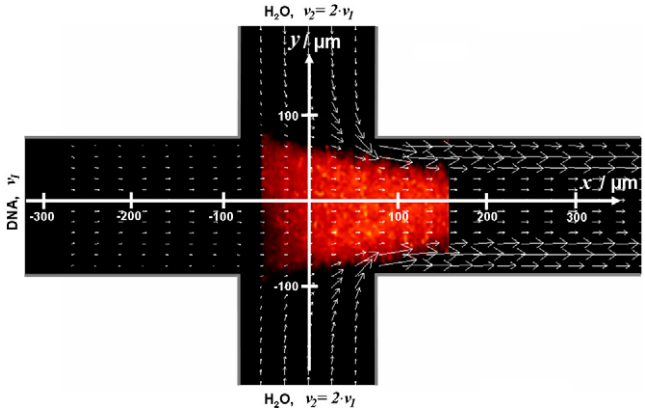

Figure 3. Confocal Raman image of the hydrodynamically focused DNA stream recorded at a fixed wavenumber of $\tilde{\nu} = 1576\ \mathrm{cm}^{-1}$ and the simulated velocity profile.

(CRL) [28, 29] are used to focus the x-ray beam down to a spot of ≈20 μm in diameter. Two-dimensional diffraction patterns of the liquid-crystalline materials at different positions within the microfluidic device can be obtained with a spatial resolution corresponding to the beam size and an exposure time of 30 s. A CCD camera with fluorescent screen is used as a detector. The resulting two-dimensional images of the diffraction patterns cover a q-range of 0.025–0.350 $\mathrm{Å}^{-1}$. The smectic layer spacing of the liquid crystal 8CB (n-octyl-4-cyanobiphenyl, Sigma-Aldrich) serves as calibration.

2.3. Confocal Raman microscopy

The hydrodynamically focused DNA solution and the interaction of DNA with the condensing reactants is imaged using confocal Raman microscopy. A CRM200 confocal Raman microscope, manufactured by WiTec (Ulm, Germany), is used for room-temperature Raman microscopy analysis of the dynamics of DNA condensation. The microscope is equipped with a piezo scanning table which can be moved (200 ± 0.004) μm in the x and y directions and (20 ± 0.001) μm in the z direction. A laser beam (SGL-2200 laser, 532 nm, Shanghai Uniwave Technology) is focused on the sample using a diffraction limited spot size by an Olympus LMPlanFl 100× objective. The measured signal is transmitted to a spectrograph via an optical fibre with a diameter of 50 μm. The end of this fibre is placed at the image plane of the microscope and used as a pinhole. The microscope provides a recording of spectra with an air-cooled CCD chip (1340 × 1000 pixels) behind a grating spectrograph with a grating of 600 lines per mm and a resolution of 6 cm^{-1}. Additionally, high-resolution 2D Raman images of the sample at fixed wavenumbers can be recorded by laterally (x–z, y–z) rasterizing the sample through the excitation spot using the scanning table and detecting the Raman signal with an avalanche photodiode detector (APD).

3. Hydrodynamic focusing and orientation of DNA molecules in semidilute solutions

Hydrodynamic focusing with an extensional flow profile is generated by a crossed microchannel device with a channel width of 150 μm. A centre stream of 10 $\mathrm{mg\,ml}^{-1}$ semidilute DNA solution with a mean velocity $v_1 = 250\ \mu\mathrm{m\ s}^{-1}$ is hydrodynamically focused by two symmetrical side streams of water with $v_2 = 2v_1$. The Raman image in figure 3

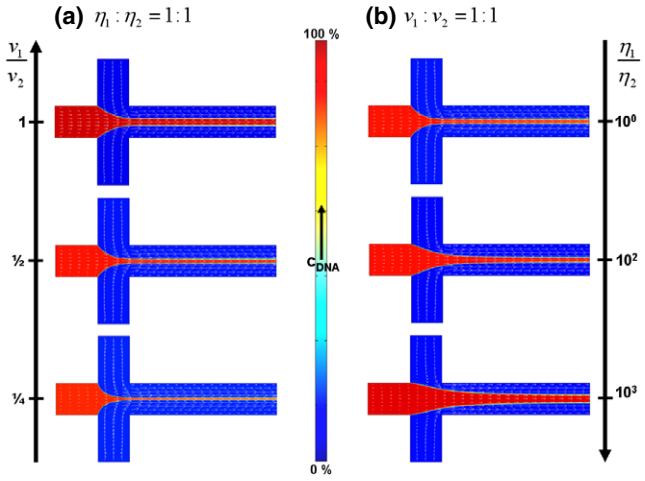

Figure 4. Simulation data of the flow profiles for different velocity ratios (a) and viscosity ratios (b).

is recorded by lateral scanning of the flow cell using the avalanche photodiode detector at a specific wavenumber of $\tilde{\nu} = 1576\ \mathrm{cm}^{-1}$. At this wavenumber, the Raman spectrum of DNA shows a prominent peak which arises from vibrations of the bases guanine and adenine. Due to self-fluorescence of semidilute DNA solutions, higher DNA concentrations are problematic when using Raman microscopy. Interestingly, the stream profile of the DNA solution shown in figure 3 displays a much broader shape than expected from the flow rate ratios used in the channels.

To understand this phenomenon, the velocity profile in the hydrodynamic focusing device is modelled using finite element method simulations and overlaid with the Raman image. The incompressible Navier–Stokes equation is solved in two dimensions (using the commercial software Femlab) to obtain a stationary solution (low Reynolds numbers using about 20 000 elements). The viscosity of the DNA solution is used as a fit parameter in the simulations to match the experimental results. Although the viscosity of a DNA solution is anisotropic, since the long, semiflexible DNA macromolecules are oriented into the direction of the flow, for simplification an isotropic viscosity of $\eta_1 \sim 10^3\eta_2 = 10^3\eta_{\mathrm{water}}$ ($\eta_{\mathrm{water}} = 0.891$ mPa s) is used. Since we are able to achieve the actual shape of the hydrodynamically focused DNA solution as shown in figure 3, the assumption of an isotropic viscosity represents an adequate approximation of the experimental situation. The anisotropy of the viscosity plays an important role when diffusive mixing of reactant into the hydrodynamically focused DNA stream is studied (see reaction of DNA with G4 in section 4).

In figure 4, modelled velocity profiles of the hydrodynamic focusing device are shown for different velocity ratios v_1/v_2 and viscosity ratios η_1/η_2 of the main channel and side channels. As expected, a parabolic velocity profile perpendicular to the flow direction can be obtained in the channels. At the confluence of the three inlet channels, the flow patterns are interfering, and focusing of the main liquid stream as well as a simultaneous acceleration of the flow can be observed. The width of the focused liquid stream can be adjusted by the ratio v_1/v_2 of the flow rates of the main channel and side channels (figure 4(a)). In figure 4(b) the simulated flow profiles for three different viscosity ratios η_1/η_2 (i.e. different DNA concentrations) at a fixed ratio $v_1/v_2 = 1/2$ are shown. Although the velocities of all three inlet channels remain unchanged, depending on the ratio of viscosity η_1/η_2 significant differences in the flow profile are observable.

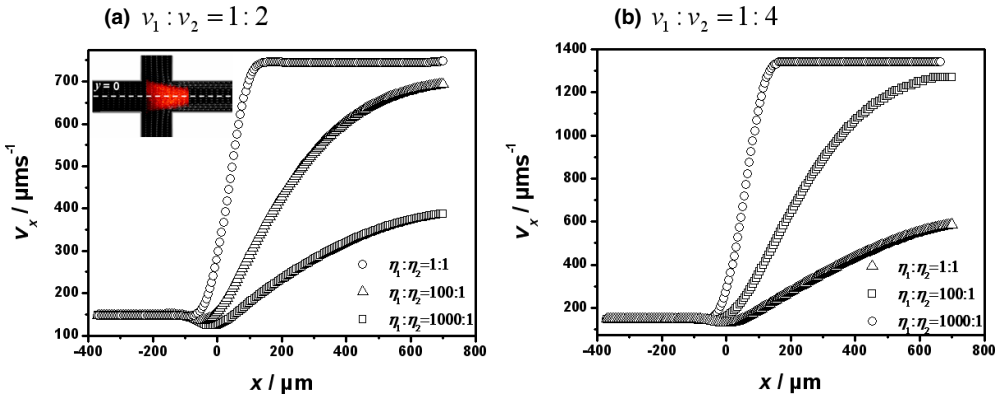

Figure 5. Dependence of the flow velocity v_x along the x-axis ($y = 0$) for different ratios of viscosities η_1/η_2 at fixed velocity ratios of $v_1/v_2 = 1/2$ (a) and $v_1/v_2 = 1/4$ (b).

For a detailed analysis, the velocity v_x along the x-axis ($y = 0$) is plotted in figure 5 for different ratios of viscosities η_1/η_2 at fixed velocity ratios of $v_1/v_2 = 1/2$ and $v_1/v_2 = 1/4$. The only difference between the velocity courses at different ratios v_1/v_2 is the absolute magnitude of v_x. Independent of the velocity ratio v_1/v_2 used, the velocity profile of the low-viscosity solution shows that acceleration occurs only in the microchannel intersection and the velocity remains constant after passing it. Yet, with increasing viscosity of the solution in the main channel the acceleration region expands significantly. Depending on the ratio of η_1/η_2, acceleration is noticeable for several 1000 μm down the outlet channel.

To experimentally analyse the influence of the velocity field on the orientation of the DNA macromolecules, a centre stream of 20 mg ml^{-1} DNA solution with a mean velocity $v_1 = 250$ μm s^{-1} was hydrodynamically focused by two symmetrical side streams of a 67% aqueous glucose solution with $v_2 = 4v_1$. The viscosity ratio of the solutions in the main and the side channels is $\eta_1 : \eta_2 \approx 1000{:}1$.

A DNA correlation peak at $q = 0.0498$ Å^{-1} is measured in the inlet channel at $x = -200$ μm using small angle x-ray microdiffraction corresponding to an interaxial spacing of $d = 126.1$ Å (figure 6(a)) [30]. Azimuthal distributions of the DNA correlation peak at different positions along the x-axis are shown in figure 6(b).

At a position of $x = -300$ μm the DNA molecules show a weak pre-elongation along the inlet channel due to the viscous flow which is highly dependent on the concentration of the DNA solution. Maximal intensity can be observed at azimuthal angles of $\chi_{\max} = -90°$ and $\chi_{\max} = 90°$. To quantify the orientation, the peaks are Gaussian fitted and the standard deviation σ from the azimuthal angle of maximum intensity is determined for and plotted in dependence of the x position (figure 6(c)).

From the simulated velocity course shown in figure 5, an orientation of the DNA molecules is expected, starting at the intersection area. Owing to the high viscosity of the DNA solution, a slight pre-orientation of the DNA molecules along the flow direction in the inlet channel far away from the intersection area ($x = -300$ μm) is observable. Starting at $x \approx -150$ μm, a continuous increase in orientation of the DNA molecules is observable due to the hydrodynamic focusing leading to a decrease of σ. According to the simulation data (figure 5), this is only expected at $x > 0$ μm. The early onset of the increase in orientation can be attributed to the entanglement of DNA molecules in semidilute solutions.

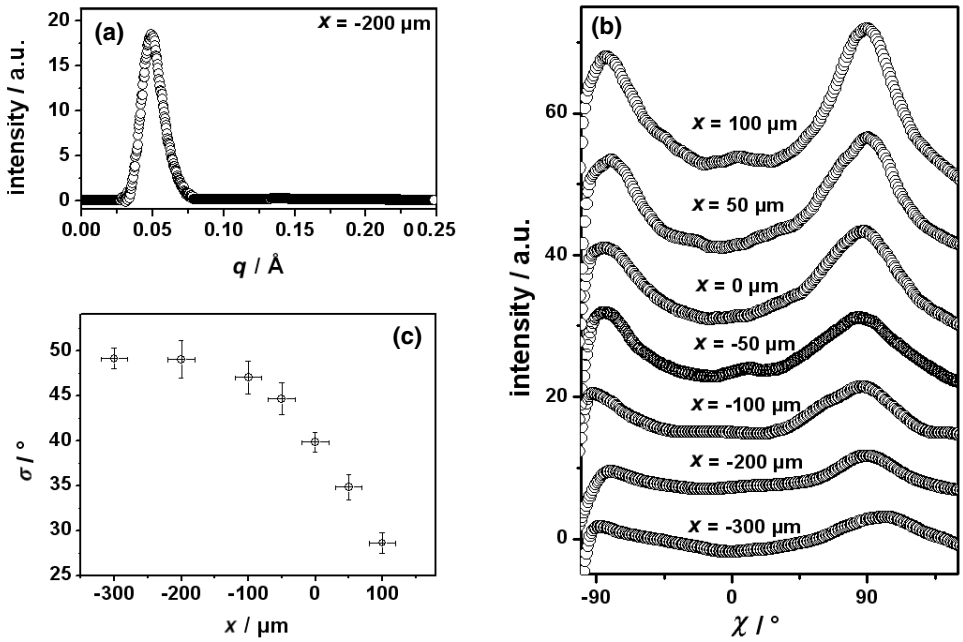

Figure 6. DNA correlation peak (a) and intensity modulation of the DNA correlation peak (scans of the azimuth angle χ) at different positions x (b). (c) Dependence of the standard deviation σ on the position along the x-axis.

4. Compaction of DNA by G4 dendrimers

As well as hydrodynamic focusing of a liquid stream, using two miscible liquids in crossed microchannels allows for diffusive mixing of these liquids. This opens a wide field of interesting experiments [27, 31]. Here, semidilute aqueous solutions of DNA (2.5–10 mg ml^{-1}) are injected in the centre channel with mean flow velocities of $v_1 \approx$ 100–300 μm s^{-1} and hydrodynamic focusing of the DNA solution is initially formed by injected pure water from the side channels. After establishing a stationary flow, G4 dendrimers are continuously added to both side streams by changing the relative pump rates of the two syringes connected to each side channel. The G4 concentration can be varied from 0 mg ml^{-1} (only water) to 10 mg ml^{-1} (only aqueous G4 solution) (figure 2). Subsequent to the intersection, the interaction of G4 with DNA can be observed along the outlet channel. Reducing the width of the focused liquid stream, and therefore the diffusion, allows for fast mixing and the observation of the evolution of interactions between the mixed compounds [20, 32].

4.1. Raman microscopy of G4/DNA interactions

Using Raman microscopy, it is possible to image the diffusion controlled interaction of G4 and DNA. The Raman spectrum of G4/DNA aggregates is largely consistent with the sum of the intensities of the corresponding Raman bands in the individual G4 and DNA spectra. However, a distinct reduction in intensity of the most prominent phosphate group bands at $\tilde{\nu} = 782$ and $\tilde{\nu} = 1087$ cm^{-1} is revealed, indicating that the negatively charged groups along

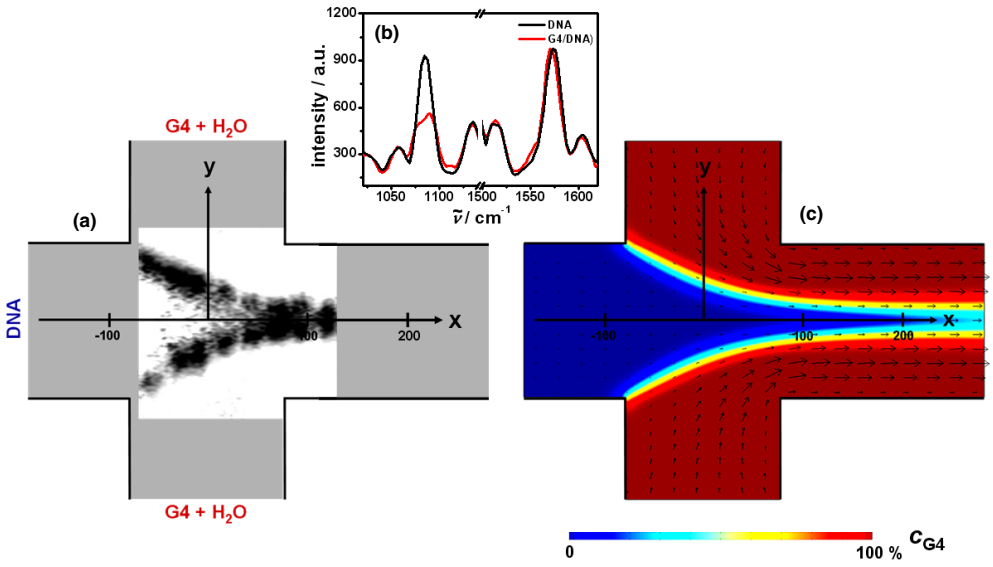

Figure 7. Monitoring the ongoing condensation of DNA by confocal Raman microscopy of the hydrodynamically focused DNA solution at fixed wavenumbers of $\tilde{\nu} = 1087\ \mathrm{cm}^{-1}$ (reaction band) and $\tilde{\nu} = 1576\ \mathrm{cm}^{-1}$ (reference band). The Raman image shown is the quotient of the Raman intensities I_{1087}/I_{1576} of the two scans (a). Raman spectrum of DNA and G4/DNA in the regions of interest (b). Simulation of the velocity profile and the concentration gradients of the experimental situation (c).

the DNA backbone are the main targets of the amine groups of the G4 dendrimers. This reflects the fact that electrostatic attraction between both molecules is the driving force for the DNA condensation [33, 34]. Here, we want to focus on the Raman band at $\tilde{\nu} = 1087\ \mathrm{cm}^{-1}$ which arises from a symmetric stretching vibration of the PO_2^- moiety and is easily distinguishable from other Raman bands of B-form DNA in its vicinity [33–35]. Being almost unaffected by aggregation, the intensity of the Raman band at $\tilde{\nu} = 1576\ \mathrm{cm}^{-1}$, which arises from vibrations of the bases guanine and adenine, can be used as reference [33]. Therefore, the reduction in intensity of the Raman bands at $\tilde{\nu} = 1087\ \mathrm{cm}^{-1}$ relative to the reference intensity of the band at $\tilde{\nu} = 1576\ \mathrm{cm}^{-1}$ can be used as benchmarks for the aggregation reactions. Comparing the intensities of the Raman band at $\tilde{\nu} = 1087\ \mathrm{cm}^{-1}$ in the DNA and the G4/DNA spectra show a reduction of 30% (figure 7(b)).

We apply this knowledge of the Raman spectrum of G4/DNA aggregates for systematic, lateral Raman imaging of the hydrodynamically focused DNA stream for these two specific wavenumbers. The Raman scans of the sample reflect the local intensities at the chosen wavenumber. The image recorded at $\tilde{\nu} = 1087\ \mathrm{cm}^{-1}$ is divided by the image obtained at $\tilde{\nu} = 1576\ \mathrm{cm}^{-1}$ and the result is displayed in figure 7(a) showing the already reacted areas. As soon as the solutions meet at the intersection of the channels, the positively charged dendrimers react with the negatively charged, elongated DNA molecules and diffuse into the DNA stream. The diffusion of long chain DNA molecules, which are elongated and preferentially oriented perpendicular to the diffusion direction, into the G4 solutions can be neglected since the mobility of the DNA macromolecules ($D_{\mathrm{DNA}} \approx 2 \times 10^{-12}\ \mathrm{m}^2\ \mathrm{s}^{-1}$ [36]) is much lower than that of G4 dendrimers ($D_{\mathrm{G4}} \approx 1.6 \times 10^{-10}\ \mathrm{m}^2\ \mathrm{s}^{-1}$, estimated from the Stokes–Einstein relation, $r_{\mathrm{G4}} = 1.6$ nm).

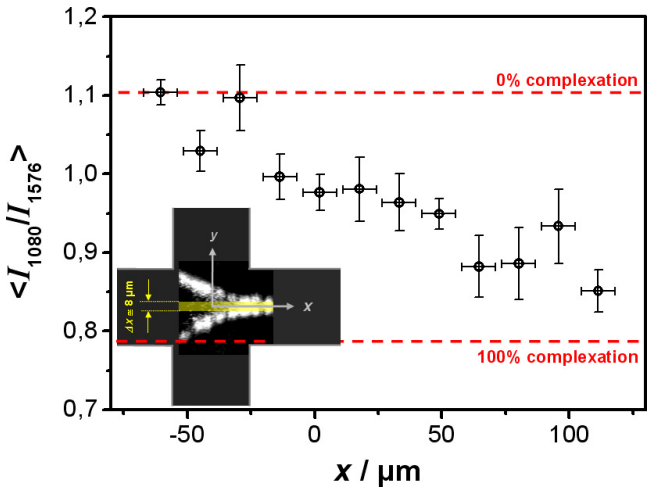

Figure 8. Monitoring the aggregation of the centre of the hydrodynamically focused DNA stream along the outlet channel. With increasing concentration of G4 molecules additional phosphate groups are complexed and the intensity ratio is reduced.

Again, simulations are used to model the experimental situation. The assumption that the anisotropy of the viscosity (see section 3) plays an important role is supported by the fact that the diffusion in our system is much faster than we would expect in an isotropic, non-reacting system. According to the Stokes–Einstein equation, the viscosity and diffusion coefficient are reciprocal [36]. This would imply that the diffusion of G4 into the DNA solution would be about three orders of magnitude slower than in a corresponding water–water system without viscosity-raising DNA. However, our experiments show that this is not the case. In contrast, the diffusion is approximately as fast as in water. This is caused by the driven reaction which leads to the formation of G4/DNA aggregates and by the anisotropy in viscosity as well as in diffusion (the Stokes–Einstein equation only applies on the assumption that the molecules are spherical). From the fact that the width of the reacted areas following the diffusion profile is constant along the outlet channel, it can be concluded that the timescale on which the condensing reaction takes place is much smaller than the diffusion timescale.

Since the whole system is dominated by laminar flow, each position along the outlet channel represents a steady state in reaction evolution. Owing to the diffusive mixing behaviour, different local concentrations exist along and perpendicular to the hydrodynamically focused DNA stream. Changes in the relative charge ratio N/P which is known to influence the structure of the aggregates formed are correlated with these concentration variations [37]. Here, N denotes the number of positive amine charges of the dendrimers (assuming full protonation) whereas P is the number of negative phosphate charges of the DNA backbone. Owing to the laminar flow and the diffusive mixing, different N/P ratios and therefore different aggregation states are observable along the outlet channel. Therefore, different time frames of the mixing reaction are accessible by varying the flow velocities and/or the observation position along the outlet channel. The local concentrations along the outlet channel can be estimated to a good approximation from the simulation data.

To study the evolution of DNA compaction by G4 dendrimers diffusing into the DNA stream, in figure 8 the ratio of mean intensities of the Raman bands at $\tilde{\nu} = 1087$ cm^{-1} and $\tilde{\nu} = 1576$ cm^{-1} in an interval $\Delta y = 8$ μm around the centre of the main channel ($y = 0$) is shown in dependence of the position along the x-axis. From Raman spectra the ratio of

intensity of the two Raman bands at $\tilde{\nu} = 1087\ \mathrm{cm}^{-1}$ and $\tilde{\nu} = 1576\ \mathrm{cm}^{-1}$ for pure (non-compacted) DNA is known to be $I_{1080}/I_{1576} \approx 1.1$. Adding G4 molecules, the negatively charged phosphate groups are complexed by positively charged dendrimeric sites and the ratio of intensity of the two bands decreases to a final value of $I_{1080}/I_{1576} \approx 0.78$. Figure 8 shows that the decrease in intensity is directly correlated with the concentration of the dendrimers. Along the outlet channel, more and more dendrimers are diffusing into the DNA stream and condensing to the negatively charged phosphate groups of the DNA backbone. The final ratio of intensity, $I_{1080}/I_{1576} \approx 0.78$, is reached at $x \approx 200\ \mu$m (figure 8). Although G4 dendrimers are continuing to diffuse into the DNA stream, the intensity ratio I_{1080}/I_{1576} remains constant, indicating that all (accessible) phosphate groups are complexed by dendrimeric amine groups. Small angle x-ray microdiffraction is used to obtain structural information about the formed G4/DNA aggregates.

4.2. Small angle x-ray microdiffraction of DNA compaction by G4 dendrimers

G4 dendrimers are known to compact DNA and generate different liquid crystalline columnar phases depending on the relative charge ratio N/P [37]. Using an x-ray beam with a diameter of 20 μm, good spatial resolution is obtained and we are able to measure the dynamics of DNA compaction in dependence on the N/P ratio by varying the observation position. Here, a centre stream of 10 mg ml^{-1} aqueous DNA solution with a mean velocity $v_{\mathrm{DNA}} \approx 100\ \mu\mathrm{m\ s}^{-1}$ is hydrodynamically focused by two symmetrical side streams of aqueous G4 solution with $v_{\mathrm{G4}} = 4v_{\mathrm{DNA}}$. The G4 concentration varys along the outlet channel, resulting in a final N/P ratio of 4. Small angle x-ray microdiffraction data for the self-assembly of the G4/DNA condensates at different positions x of the mixing and interaction area of the microfluidic device are shown in figure 9.

The peak at $q_0 = 0.1945\ \mathrm{Å}^{-1}$ which is emerging at $x = 200\ \mu$m corresponds to a liquid crystalline columnar mesophase with a spacing of $d = 2\pi/q_0 = 32.3$ Å. The peak shows an asymmetrical profile but owing to the absence of higher-order peaks the detailed structure cannot be elucidated. Moving the spatial position down the outlet channel to $x = 700\ \mu$m, a more prominent peak can be observed at $q_0 = 0.1868\ \mathrm{Å}^{-1}$. Furthermore, a weaker second peak arises at $q_1 = 0.2619\ \mathrm{Å}^{-1} \approx \sqrt{2}q_0$ corresponding to a columnar mesophase with an in-plane square symmetry. In analogy to bulk experiments [37], a phase transition from a columnar mesophase with probably hexagonal in-plane structure to a mesophase with a two-dimensional square structure can be found with increasing N/P ratio. Moving the observation position to larger x, the spacing of the columnar in-plane square symmetry increases to $d = 34.5$ Å due to additional G4 molecules condensing into the compacted DNA aggregates.

The elongated flow leads to an orientation of the self-assembling materials. Scans of the azimuthal distribution, χ, of the intensity of the q_0-peaks at different x positions are shown in figure 9(b). A strong orientation of G4/DNA aggregates is observable along the flow direction which corresponds to maximum intensities of azimuthal angles at $\chi_{\max} = -90°$ and $\chi_{\max} = 90°$. Maximum orientation is achieved at the position $x = 1500\ \mu$m. Moving to larger x, the orientation of the DNA condensates is becoming weaker, but still exists at $x = 3000\ \mu$m. This is in good agreement with the simulations for differing viscosities η_1 and η_2 shown in figure 5. Dependent on the ratio of η_1/η_2, the applied stress owing to the confluence of the inlet streams can be experienced up to several 1000 μm down the outlet channel. The observed decrease in intensity in figure 9 for $x = 3000\ \mu$m is puzzling. A possible explanation could be that due to the increasing dendrimer concentration a dissolution of the formed complexes takes place, leading to a decrease in intensity. Furthermore, experimental inadequacies could result in the fact that the x-ray beam is no longer fully hitting the hydrodynamic focused DNA jet.

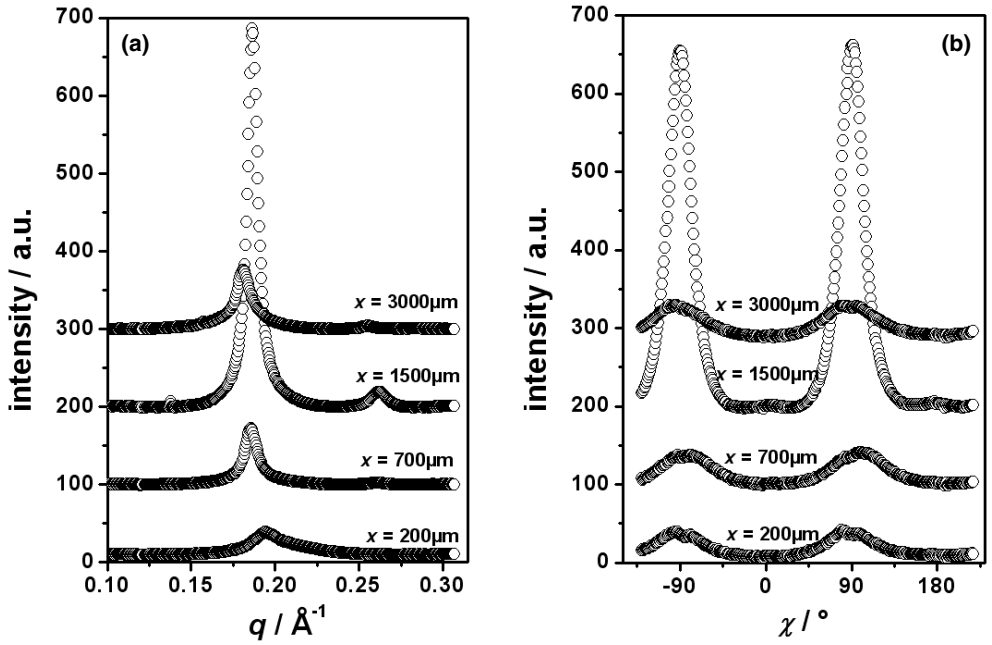

Figure 9. Series of small angle x-ray microdiffraction measurements of the self-assembled G4/DNA condensates (a) and intensity modulation in dependence on the azimuth angle χ at different positions along the outlet channel (b).

Comparing this structural information with the Raman data, the development from a liquid crystalline columnar mesophase with weakly correlating in-plane structure to one with quadratic in-plane symmetry can be assigned to increased complexation of the negatively charged phosphate groups by dendrimeric amine groups along the outlet channel. The complexation of all (accessible) phosphate groups could correspond to the (full) emergence of the columnar mesophase with the in-plane square symmetry showing a well-defined structural order. As expected from Raman analysis, additional G4 molecules diffuse into the DNA stream along the outlet channel leading to the observed change in spacing of the columnar in-plane symmetry from $d = 32.3$ to 34.5 Å.

5. Conclusions

To summarize, employing chemically sensitive Raman microscopy, the molecular interactions of DNA with G4 dendrimers were studied and the results combined with structural information resulting from small angle x-ray microdiffraction measurements, allowing for a detailed insight into the characteristics and the evolution of self-assembled supramolecular dendrimer/DNA structures. The phase transition towards a columnar mesophase with an in-plane square symmetry was monitored in dependence of the N/P ratio. On a molecular level, the onset of the square columnar mesophase corresponds to a complete complexation of all (accessible) DNA phosphate groups by dendrimeric amine sites. Inducing alignment by hydrodynamic focusing of the condensed structures in microfluidic devices led to an improved characterization of the G4 dendrimer/DNA aggregates and the effect of hydrodynamic stress on the macromolecules could be tested. The diffusive mixing in the microchannels provided very defined and controllable reaction conditions with changing local concentration along the outlet

channel enabling the study of the dynamics of the ongoing G4/DNA interactions. Additional information about the acceleration and the variation of local concentrations was provided by modelling the velocity profile of the hydrodynamic focusing device using the finite element method.

Acknowledgments

We gratefully acknowledge useful discussions with Stephan Herminghaus, Dagmar Steinhauser, Heather Evans, Anatoly Snigirev and Oleg Konovalov. We thank Udo Krafft for his help in developing the microsyringe system, and the machine shops of the University of Ulm and the MPI for Dynamics and Self-Organization for spark eroding of the steel plates. We acknowledge the European Synchrotron Radiation Facility for provision of synchrotron radiation facilities at beamline ID10b. This work was supported by the DFG within the Emmy-Noether-Programme (Pf 375/2).

References

[1] Minsky A, Shimoni E and Frenkiel-Krispin D 2002 *Nat. Rev. Mol. Cell Biol.* **3** 50
[2] Wojtuszewski K, Hawkins M E, Cole J L and Mukerji I 2001 *Biochemistry* **40** 2588
[3] Davey C A, Sargent D F, Luger K, Maeder W and Richmond T J 2002 *J. Mol. Biol.* **319** 1097–113
[4] Bohrmann B, Haider M and Kellenberger E 1993 *Ultramicroscopy* **49** 235
[5] Tzlil S, Kindt J T, Gelbart W M and Ben-Shaul A 2003 *Biophys. J.* **84** 1616
[6] Odijk T 1998 *Biophys. J.* **75** 1223
[7] Wagner K, Harries D, May S, Kahl V, Rädler J O and Ben-Shaul A 2000 *Langmuir* **16** 303
[8] Mel'nikov S M, Sergeyev V G, Yoshikawa K, Takahashi H and Hatta I 1997 *J. Chem. Phys.* **107** 6917
[9] Kötz J, Köpke H, Schmidt-Naake G and Vogl O 1996 *Polymer* **37** 2775
[10] Rau D C and Parsegian V A 1992 *Biophys. J.* **61** 246
[11] Raspaud E, Olvera de la Cruz M, Sikorav J L and Livolant F 1998 *Biophys. J.* **74** 381
[12] Jansen J F, de Brabander-van den Berg E M and Meijer E W 1994 *Science* **266** 1226
Frey H, Lorenz K, Holter D and Mulhaupt R 1996 *Polym. Prepr.* **37** 758
[13] Kabanov V A, Sergeyev V G, Pyshkina O A, Zinchenko A A, Zezin A B, Joosten J G H, Brackman J and Yoshikawa K 2000 *Macromolecules* **33** 26
[14] Kukouska-Latallo J F, Bielinsk A U, Johnson J, Spindler R, Tomalia D A and Baker J R 1996 *Proc. Natl Acad. Sci.* **93** 4897
[15] Braun C S, Vetro J A, Tomalia D A, Koe G S, Koe J G and Middaugh C R 2005 *J. Pharm. Sci.* **94** 423
[16] Dennig J and Duncan E 2002 *Rev. Mol. Biotechnol.* **90** 339
[17] Pack D W, Hoffman A S, Pun S and Stayton P S 2005 *Nat. Rev. Drug Disc.* **4** 581
[18] Beebe D J, Mensing G A and Walker G M 2002 *Annu. Rev. Biomed. Eng.* **4** 261
[19] Hansen C and Quake S R 2003 *Curr. Opin. Struct. Biol.* **13** 538
[20] Pollack L, Tate M W, Darnton N C, Knight J B, Gruner S M, Eaton W A and Austin R 1999 *Proc. Natl Acad. Sci.* **96** 10115
[21] Schroeder C M, Babcock H P, Shaqfeh E S G and Chu S 2003 *Science* **301** 1515
[22] Pfohl T, Mugele F, Seemann R and Herminghaus S 2003 *Chem. Phys. Chem.* **4** 1291
[23] Hud N V and Downing K H 2001 *Proc. Natl Acad. Sci.* **98** 14925
[24] Golan R, Pietrasanta L I, Hsieh W and Hansma H G 1999 *Biochemistry* **38** 14069
[25] Struth B, Snigirev A, Konovalov O, Otten A, Gauggel R and Pfohl T 2003 *AIP Conf. Proc. SRI 2003* **705** 804
[26] Kumar A and Whitesides G M 2002 *Appl. Phys. Lett.* **1993** 63
[27] Otten A, Köster S, Struth B, Snigirev A and Pfohl T 2005 *J. Synchrotron Radiat.* **12** 745
[28] Snigirev A, Kohn V, Snigireva I and Lengeler B 1996 *Nature* **384** 49
[29] Lengeler B, Schroer C G, Benner B, Gerhardus A, Günzler T F, Kuhlmann M, Meyer J and Zimprich C 2002 *J. Synchrotron Radiat.* **9** 119
[30] Durand D, Doucet J and Livolant F 1992 *J. Physique* II **2** 1769
[31] Otten A, Köster S, Dootz R, Struth B and Pfohl T 2006 submitted
[32] Knight J B, Vishwanath A, Brody J P and Austin R H 1998 *Phys. Rev. Lett.* **80** 3863
[33] Deng H, Bloomfield V A, Benevides J M and Thomas G J Jr 2000 *Nucl. Acids Res.* **28** 3379

[34] Deng H, Bloomfield V A, Benevides J M and Thomas G J Jr 1999 *Biopolymers* **50** 656
[35] Guan Y, Choy G S-C, Glaser R and Thomas G J Jr 1995 *J. Phys. Chem.* **99** 12054
[36] Atkins P W 1998 *Physical Chemistry* (Oxford: Oxford University Press)
[37] Evans H M, Ahmad A, Ewert K, Pfohl T, Martin-Herranz A, Bruinsma R F and Safinya C R 2003 *Phys. Rev. Lett.* **91** 7